Surface-Enhanced Raman Scattering Study on Graphene-Coated Metallic Nanostructure Substrates

Qingzhen Hao[1,2], **Bei Wang**[2], **Jeremy A. Bossard**[3], **Brian Kiraly**[1], **Yong Zeng**[3], **I-Kao Chiang**[1], **Lasse Jensen**[4], **Douglas H. Werner**[3], and **Tony Jun Huang**[1,*]

[1]Department of Engineering Science and Mechanics, The Pennsylvania State University, University Park, PA 16802

[2]Department of Physics, The Pennsylvania State University, University Park, PA 16802

[3]Department of Electrical Engineering, The Pennsylvania State University, University Park, PA 16802

[4]Department of Chemistry, The Pennsylvania State University, University Park, PA 16802

Abstract

Graphene, which has a linear electronic band structure, is widely considered as a semimetal. In the present study, we combine graphene with conventional metallic surface-enhanced Raman scattering (SERS) substrates to achieve higher sensitivity of SERS detection. We synthesize high-quality, single-layer graphene sheets by chemical vapor deposition (CVD) and transfer them from copper foils to gold nanostructures, *i.e.*, nanoparticle or nanohole arrays. SERS measurements are carried out on methylene blue (MB) molecules. The combined graphene nanostructure substrates show about threefold or ninefold enhancement in the Raman signal of MB, compared with the bare nanohole or nanoparticle substrates, respectively. The difference in the enhancement factors is explained by the different morphologies of graphene on the two substrates with the aid of numerical simulations. Our study indicates that applying graphene to SERS substrates can be an effective way to improve the sensitivity of conventional metallic SERS substrates.

Keywords

Graphene; SERS; Plasmonics; Nanostructure

1. Introduction

Surface-enhanced Raman scattering (SERS)[1, 2] can increase the cross section of Raman scattering, matching or even exceeding that of linear Rayleigh scattering through a combination of metal-molecule chemical effects and intense enhancement of localized electromagnetic fields around metallic nanostructures.[3, 4] SERS is currently the only method capable of simultaneously detecting a single molecule and providing its chemical fingerprint.[5] This method has the potential for high impact on biochemical sensing, such as

---

[*]Author to whom correspondence should be addressed. junhuang@psu.edu.

DNA and bacterial detection,[6–9] real-time glucose sensing for diabetes,[10, 11] and *in situ* identification of reaction products.[12, 13] SERS has been transformed into a powerful analytic technique, especially in recent years, due to advances in nanofabrication and increased understanding of the plasmonic properties of nanomaterials.[14–20] A host of nanoparticle or nanohole substrates have been demonstrated with promising SERS sensitivities.[21–26] SERS can also be integrated with microfluidic components to enable fully integrated biosensing systems.[27–34]

Graphene, a single sheet of carbon atoms, has an ideal 2D honeycomb crystal structure.[35] Extensive π electron conjugation and delocalization give rise to the extreme physical strength and chemical inertness of graphene. Moreover, graphene is biocompatible and has been demonstrated to be an excellent bio-sensing material.[36–38] Most of these applications are based solely on the transport properties of graphene. However, graphene also has other interesting properties. For example, mechanically exfoliated graphene and its chemical derivative serving as SERS substrates have recently been demonstrated to offer signal enhancement due to a chemical mechanism.[39–46] It has also been shown that graphene can reduce the "SERS background"[47] or quench molecule fluorescence to improve Raman signal-to-noise ratio (S/N).[48, 49]

Here, we present a SERS study on graphene coated nanostructures, *i.e.*, nanohole and nanoparticle arrays, using methylene blue (MB) as the probe molecule. High-quality, single-layer graphene (SLG) was synthesized by chemical vapor deposition (CVD) on copper foil and transferred to the substrates with gold nanostructures. SERS measurements were then carried out and compared among different substrates. Bare graphene is shown to enhance the Raman signal of MB by a factor of ~16. The combined graphene nanostructure substrates show about threefold or ninefold enhancement in the Raman signal of MB compared to bare nanohole or nanoparticle substrates, respectively. The SERS enhancement mechanism of the SLG-coated substrates is discussed, and the different enhancement factors (EFs) between graphene coated nanoparticles and nanoholes are understood based on the different morphologies of graphene on the two substrates using numerical simulation.

2. Experimental Details

Graphene Synthesis by CVD

Following the method introduced by Ruoff's group,[50] we synthesize high-quality graphene on copper foil (Alfa Aesar 25 μm thick) using low-pressure CVD. It is known that CVD growth of graphene on a copper surface is a self-saturation process, which produces mainly single-layer graphene.[50, 51] The copper foil is first cleaned by dilute hydrochloric acid for 5 min to remove the copper oxide. Then the foil is annealed in the forming gas (H_2 10% / Ar) at 600 °C for 10 min and at 900 °C for another 10 min at ambient pressure. This annealing step is believed to increase the surface domain size of copper.[51] Methane gas is introduced at 1000°C when the pressure is pumped down to ~300 mTorr. The methane gas flows for 15 min, after which the system cools down naturally.

Graphene Transfer

Polymethyl methacrylate (PMMA) is used to assist the transfer of synthesized graphene from the copper foil to the nanostructures. A PMMA layer of ~300 nm in thickness is first spin-coated onto the graphene-covered copper foil. The copper foil is then etched away by copper etchant CE-100 (Transene). The PMMA film with graphene is washed three times in deionized water and fished out from the water using the substrate with nanostructures. Finally, the PMMA is chemically dissolved by Remover PG (MicroChem) at 40 °C followed by room-temperature Remover PG and IPA rinsing. The substrate is then dried naturally. Using this method we can transfer graphene onto either the nanohole or nanoparticle substrates.

SERS Measurement

The nanostructure SERS substrates are incubated in a 1×10^{-4} mol/L MB ethanol solution for ten min, then rinsed by the solvent and dried under nitrogen gas flow. Atomic Force Microscope (AFM) measurements indicate MB molecules fully cover the substrate surface (See Fig. S1 in the Supplementary Information). By saturating the SERS substrates, we minimize the effects of molecule nonuniformities among different substrates, and thus a fair comparison of SERS enhancement can be drawn. SERS spectra are recorded using a Renishaw inVia confocal microRaman spectrometer with a $100 \times$ objective (NA = 0.95). The laser spot is less than 1 μm.

3. Results and Discussion

3.1. Characterization of SLG and SLG-Nanostructure Composite

Figure 1(a) shows the copper surface after growth, where single-layer graphene fully covers the surface with occasional multilayer dots (darker regions), as confirmed by Raman spectroscopy. The absence of an observable D band in the Raman spectrum suggests that we have high-quality graphene (see Fig. S2 in the Supplementary Information for the Raman spectrum of as-grown graphene on copper).

Nanoparticle and nanohole arrays are fabricated by electron beam lithography (EBL) followed by a special dual peel-off process to produce complementary structures as described in Ref. 52. Figure 1(b) and 1(c) show typical SEM images of graphene transferred onto the nanohole and nanoparticle arrays, respectively. The nanoparticle array is on a Si wafer with a 290 nm thermal SiO_2 layer, while the nanohole array is on a glass substrate. The nanoparticle and nanohole arrays are arranged in a square lattice (lattice constant ~ 300 nm). Each particle or hole is circular in shape with a diameter of ~ 125 nm and a height of 30 nm. The graphene that was transferred onto the nanohole arrays is well supported with no significant bends, as observed under SEM. A typical Raman spectrum of graphene on the nanohole array is shown in Fig. 1(d). In addition to the G and 2D bands, a very small D band is also observed. The intensity ratio of I_D/I_G is in the range of 0~10%, indicating that the graphene is of high quality. The graphene transferred onto the nanoparticle array, in contrast, has a different morphology, as shown in Fig. 1(c). Graphene on the glass surface alone is flat and continuous, but the graphene breaks into islands on the nanoparticles with an average size of ~2 μm and ~200 nm gaps between islands. The graphene conforms to the

top surface of nanoparticles, but droops down between the nanoparticles, adhering to the SiO$_2$ surface. Wrinkles are also formed along the lattice direction within each island (inset of Fig. 1(c)). A similar structure has been observed previously.[53] We believe the wrinkled and cracked structure is formed in the following way: While the isopropanol (IPA) dries in the last step of graphene transfer, the graphene starts to stretch itself to conform to the underlying nanoparticle topology. Once the strain reaches a critical point, the graphene sheet breaks into pieces. It has been shown that graphene synthesized by CVD is polycrystalline with mechanically weaker grain boundaries. When CVD graphene is under tension, it breaks along domain boundaries.[54, 55] Therefore, we presume that the gapping observed among islands of graphene occurs along domain boundaries.

3.2. SERS Measurement on SLG-Nanostructure Composite

The SERS functionality of the SLG-nanostructure composite is studied by measuring the enhanced Raman signal from the graphene. The laser line of 647 nm is chosen to match the localized surface plasmon resonances (LSPRs) of the nanostructures (see Fig. 5) for all the SERS measurements. Graphene on nanoholes or nanoparticles experiences a larger SERS enhancement of ~ 20 as compared to that on a continuous Au film or glass, respectively. A second order enhancement has also been observed in systems consisting of exfoliated graphene with a 4 nm Ag film or Au nanoparticles.[56, 57] No apparent D band is observed for graphene on a SiO$_2$ surface or on Au nanoholes, but the D band starts to appear for graphene on nanoparticles due to the presence of edges within the laser probe (Fig. 1(c)).

Methylene blue (MB) has been found to offer promising applications in the eradication of viruses and treatment of inoperable esophageal tumors and urinary tract infections.[58] High uptake of MB in cancerous cell cultures has also been observed.[59] We, therefore, choose MB as a probe molecule to measure the SERS performance of the SLG-nanostructure composite. The spectra presented in comparisons are obtained under the same conditions. The enhancement factor, EF, is calculated by the intensity ratio of Raman peaks of interest between different substrates.

The gap between the highest occupied energy (HOMO) level and lowest unoccupied energy (LUMO) level of MB is about 1.87 eV (664 nm).[60] Resonance Raman happens with a 647 nm laser (1.91 eV). Raman peaks of MB molecules span from 445 cm^{-1} to 1621 cm^{-1} with different vibrational symmetries (see Ref. 60 for peak assignment). All of the EFs are based on the 1621 cm^{-1} peak intensity. Schematics in Fig. 3(a) illustrate the configuration of the system. Figure 3(b) shows a Raman mapping of integrated 1621 cm^{-1} MB peak intensity superimposed on the optical image of the nanohole array. Even though graphene is not visible in the optical image without interference contrast from SiO$_2$/Si, a clear difference can be seen in the Raman mapping between nanoholes covered with or without graphene. The effects of graphene are further explored by comparing different areas of the sample containing: bare glass, graphene covered glass, Au nanoholes, and graphene covered nanoholes, as shown in Fig. 3(c). Compared to a pure glass surface, graphene enhances the MB signal by a factor of ~16. Even for 514 nm and 785 nm excitations, which are away from the absorption peak of MB, the enhancement from graphene can still be observed (see Fig. S3 in the Supplementary Information for the spectra). The EFs are very different for

different peaks, possibly due to the specific symmetry of the vibrations (See Fig. 3(d)). These observations are consistent with other reports found in the literature.[39]

The Au nanoholes, due to their large, enhanced, near-field localization, are found to give an EF of ~40. One might expect that molecules enhanced by graphene will be simultaneously enhanced by the nanoholes, providing a combined graphene-nanohole EF ~600. However, we found that coating the nanoholes with graphene yields only about a threefold additional enhancement, which gives an overall EF of ~120. In contrast to the case of the nanoholes, the graphene coating provides about a ninefold additional enhancement in the MB intensity for nanoparticles, as shown in Fig. 4. This ninefold enhancement is smaller than the potential sixteen-fold enhancement from graphene on bare glass, but it is significantly improved from the threefold enhancement from graphene on nanoholes. These different enhancements are discussed later.

3.3. SERS Enhancement Mechanism

Two widely accepted mechanisms for SERS are the electromagnetic mechanism (EM) and the chemical mechanism (CM).[3] The EM is based on the enhancement of the local electromagnetic field upon resonance excitation of LSPRs. The enhancement is roughly proportional to $|E|^4$. The CM, on the other hand, is based mainly upon a partially resonant charge transfer between the molecules and the substrate (usually metal) as well as a nonresonant chemical interaction between the ground state of the molecule and metal. In other words, the CM effect originates from the interaction between molecules and substrates.

The SERS enhancement resulting from graphene is believed to be a chemical effect.[61] When MB molecules are deposited on graphene, they orient themselves parallel to the surface of the graphene due to the π-π stacking. This configuration makes the distance between the molecules and graphene very small, making direct charge transfer between graphene and the molecules much easier. Previous research has already shown that charge transfer can occur between graphene and certain molecules. [62] Charge transfer is usually thought to be a "first-layer effect"; that is, a short-range effect occurring on the molecular scale such that the wave function of the molecule and metal can overlap. Recently, experimental evidence[63] shows that enhancement from graphene mainly comes from the first monolayer of probe molecules, rather than from subsequent layers, and that Raman enhancement depends on the molecular configuration in contact with the graphene. These results reveal that graphene enhancement is strongly dependent on the distance between graphene and the molecules; there is strong evidence that the SERS effect due to graphene belongs to a chemical enhancement mechanism.

Our previous study shows that the CM effect in SERS is governed by the energy difference between the Fermi-level of the metal and the LUMO of the molecule.[64] This implies that the molecules that show significant stabilization of the HOMO-LUMO gaps (such as those readily accepting π-backbonding) are likely to have strong CM enhancements. Due to the strong π-π interactions between MB molecules and the graphene substrate, we would expect the CM effect to be strong for the graphene system. This is further supported by the handful

of experimental papers reporting on SERS studies using graphene, which adapts a variety of molecules with significant π-π interactions.[39, 40, 63, 65]

On the other hand, EM is well accepted as the main mechanism of SERS for metallic nanostructures. The local electric field near the nanostructure is greatly enhanced by its LSPRs, which produce an enhancement that is highly localized to the metal surface.[66] The CM only contributes a minor enhancement compared with the EM for metal substrates. In the end, the two enhancement mechanisms are combined to give the overall SERS enhancement. For graphene-coated nanostructures, the stronger chemical enhancement from graphene can potentially be used to improve the SERS enhancement of bare Au nanostructures.

3.4. Effects of SLG on Nanostructure Properties

It has been shown that LSPRs can be excited in optically thin metal films perforated with subwavelength holes or their nanoparticle counterparts.[67–71] For a nanohole array, a resonance can be observed by a peak in the transmission spectrum (Fig. 5(a)), which occurs at ~680 nm for our structure.[52] The peak at ~500 nm is from the continuous part of the Au film. The graphene-covered nanoholes show a similar transmission spectrum with a slightly reduced intensity. A relative reflection measurement (w.r.t. the Si wafer) is used to measure the LSPRs of the nanoparticles on a silicon wafer, as shown by the minimum in the spectra in Fig. 5(b). Since the nanoparticle array is complementary to the nanohole array, its resonance position is also around 680 nm. The "double-dip" feature (as indicated by the arrows) in the relative reflection spectra is due to interference from the 290 nm SiO_2 layer.[72] The graphene-covered nanoparticles also have similar resonance positions, but show a small change in intensity. Due to its low free electron density, graphene doesn't support surface plasmons in the visible region as it does in the terahertz region. Its ultrathin thickness, ~ 0.335 nm, and high transparency, > 95%, make it a negligible "dielectric" layer, as confirmed in later simulations (Fig. 6). Therefore, the resonance wavelength of the SLG-nanostructure composite remains at about the same position as that of the bare nanostructure although with slightly lower transmission intensity.

Using full-wave electromagnetic simulations, we investigated the effects of the graphene coating on the plasmon resonances and analyzed the electric field distribution surrounding the nanostructures. Similar results were found for both the nanoparticle and nanohole arrays, but only the simulation results of the nanoholes are given here (See Fig. S4 in Supplementary Information for the simulation of nanoparticle array). The scattering parameters and field distributions for the nanoparticle or nanohole arrays were calculated using a periodic finite-element boundary integral (PFEBI) technique, [73] which operates on a single unit cell and enforces periodic boundary conditions for the two dimensions in the plane of the nanostructure. In the simulation, the nanostructures are illuminated by a plane wave incident from the z-direction normal to the surface with the electric field polarized in the y-direction. The permittivity of the Au film was calculated from a Lorentz-Drude model fitted to measured data, [57] while the underlying glass surface was modeled as a half- space with a non-dispersive refractive index (n = 1.46). For the graphene-coated nanoholes, a homogeneous layer of thickness 0.335 nm with an effective dielectric constant measured

using ellipsometry and fitted to a Lorentz-Drude model[57] is added to the top surface of the nanoholes, as shown in Fig.6(a). The graphene coating doesn't appear to change the plasmon resonance associated with the bare nanoholes significantly, but smaller transmission intensity is predicted, which is consistent with the experimental measurement (Fig. 5(a)). The electric field distributions calculated 1 nm above the Au surface for a 660 nm incident wave show quite similar dipolar behavior for both cases with and without graphene (Fig. 6 (c)). However, the total electric field intensity ($|E|^2$) enhancement for graphene-coated nanoholes decreases to 91% of that from bare nanoholes. The slightly reduced transmission intensity and electric field enhancement is due to the additional effective dielectric loss introduced by the graphene layer (*epsiv;*$_{SLG} \approx 5.898 + i8.292$ at 660 nm). However, since the graphene thickness is much smaller than its skin depth at 660 nm, only a small influence on the simulation is to be expected. Overall, graphene will not alter the EM enhancement from such nanostructures significantly, but could offer additional CM enhancement to improve the total SERS properties.

Additionally, the enhanced electric field decreases nearly exponentially away from the metal surface (Fig. 6(d)), making the SERS EF of metal nanostructures highly sensitive to the distance between molecules and metal surface. Graphene coating increases the separation between molecules and metal surface and slightly lowers the EM effect from the nanostructures. In the case of the nanoholes, introducing graphene also seals the nanoholes, preventing MB molecules from attaching to their inner walls. Moreover, introducing graphene decreases the EM enhancement to about 80% of the EF without graphene, considering that the enhancement is roughly proportional to $|E|^4$. However, our results show that those small decreases in the EM enhancement are compensated by the strong CM enhancement from graphene. Thus, a threefold increase in Raman signal of MB is observed after coating Au nanoholes with graphene, despite the disadvantage of graphene preventing MB molecules from attaching to the inner wall of nanoholes. The graphene on the nanoparticles, conversely, has an advantage in that it conforms fully to the particle top surface and partially to the particle side walls (Fig. 1(c)). Hence, the MB molecules have a larger probability to be enhanced by both the nanoparticles and the graphene, and a ninefold SERS increase is observed after graphene coating.

4. Conclusion

In summary, we synthesize high-quality graphene sheets and coat them onto surface-enhanced Raman scattering (SERS) substrates, *i.e*., metallic nanoparticle or nanohole arrays. Graphene adopts different morphologies on the two types of substrates. Methylene blue was used to study the SERS response of the combined system. Graphene alone was shown to enhance the Raman signal of MB by a factor of ~16, due to its chemical enhancement. Graphene does not alter the plasmonic properties of nanostructures significantly, and consequently there is little influence on the electromagnetic SERS enhancement. However, graphene offers additional chemical enhancement, which could potentially be multiplicatively combined with the normal SERS enhancement of bare Au nanostructures. The combined graphene nanostructure substrates show about threefold or ninefold enhancement in the Raman signal of MB as compared with the bare nanohole or nanoparticle substrates, respectively. We believe that the application of graphene to SERS is

not only important for studying the basic properties of both graphene and SERS, but also offers a potential way to further improve the sensitivity of conventional metallic SERS substrates, especially for those molecules with stabilized π-π backbonding.

Supplementary Material

Refer to Web version on PubMed Central for supplementary material.

Acknowledgments

References

1. Fleischmann M, Hendra PJ, Mcquillan AJ. Chem Phys Lett. 1974; 26:163.
2. Burstein E, Chen YJ, Chen CY, Lundquist S, Tosatti E. Solid State Commun. 1979; 29:567.
3. Jensen L, Aikens CM, Schatz GC. Chem Soc Rev. 2008; 37:1061. [PubMed: 18443690]
4. Lombardi JR, Birke RL. J Phys Chem C. 2008; 112:5605.
5. Kneipp K, Wang Y, Kneipp H, Perelman LT, Itzkan I, Dasari R, Feld MS. Phys Rev Lett. 1997; 78:1667.
6. Kneipp K, Kneipp H, Kartha VB, Manoharan R, Deinum G, Itzkan I, Dasari RR, Feld MS. Phys Rev E. 1998; 57:R6281.
7. Barhoumi A, Zhang D, Tam F, Halas NJ. J Am Chem Soc. 2008; 130:5523. [PubMed: 18373341]
8. Kim NH, Lee SJ, Moskovits M. Nano Lett. 1010; 10:4181. [PubMed: 20863079]
9. Huang TJ, Liu M, Knight LD, Grody WW, Miller JF, Ho C. Nucleic Acids Res. 30:e55. [PubMed: 12060693]
10. Camden JP, Dieringer JA, Zhao J, Van Duyne RP. Acc Chem Res. 2008; 41:1653. [PubMed: 18630932]
11. Lyandres O, Yuen JM, Shah NC, Van Duyne RP, Walsh JT, Glucksberg MR. Diabetes Technol The. 2008; 10:257.
12. Zhong QL, Wang XC, Zhang L, Zhang XH, Xiang J, Ren B, Tian ZQ. Acta Chim Sinica. 2003; 61:1960.
13. Rusciano G, De Luca AC, D'Alessio A, Minutolo P, Pesce G, Sasso A. Carbon. 2008; 46:335.
14. Kneipp, K.; Moskovits, M.; Kneipp, H. Springer; Berlin: 2006. p. 19-45.
15. Juluri BK, Chaturvedi N, Hao Q, Lu M, Velegol D, Jensen L, Huang TJ. ACS Nano. 2011; 5:5838. [PubMed: 21692473]
16. Zhang B, Zhao Y, Hao Q, Kiraly B, Khoo IC, Chen S, Huang TJ. Opt Exp. 2011; 19:15221.
17. Si G, Zhao Y, Liu H, Teo SL, Zhang M, Huang TJ. Appl Phys Lett. 2011; 99:033105.
18. Juluri BK, Zheng YB, Ahmed D, Jensen L, Huang TJ. J Phys Chem C. 2008; 112:7309.
19. Juluri BK, Lu M, Zheng YB, Jensen L, Huang TJ. J Phys Chem C. 2009; 113:18499.
20. Zheng YB, Juluri BK, Jensen LL, Ahmed D, Lu M, Jensen L, Huang TJ. Adv Mater. 2010; 22:3603. [PubMed: 20665562]
21. Hao Q, Juluri BK, Zheng YB, Wang B, Chiang IK, Jensen L, Crespi V, Eklund PC, Huang TJ. J Phys Chem C. 2010; 114:18059.
22. Chan CY, Xu JB, Waye MY, Ong HC. Appl Phys Lett. 2010; 96:033104.
23. Zheng YB, Payton JL, Chung C, Liu R, Cheunkar S, Pathem BK, Yang Y, Jensen L, Weiss PS. Nano Lett. 2011; 11:3447. [PubMed: 21749070]

24. Le F, Brandl DW, Urzhumov YA, Wang H, Kundu J, Halas NJ, Aizpurua J, Nordlander P. ACS Nano. 2008; 2:707. [PubMed: 19206602]

25. Fang YR, Wei H, Hao F, Nordlander P, Xu HX. Nano Lett. 2009; 9:2049. [PubMed: 19391601]

26. Hao Q, Zeng Y, Juluri BK, Wang X, Kiraly B, Chiang I, Jensen L, Werner DH, Crespi VH, Huang TJ. ACS Nano. 2011; 5:5472. [PubMed: 21657215]

27. Mao X, Waldeisen JR, Huang TJ. Lab Chip. 2007; 7:1260. [PubMed: 17896008]

28. Mao X, Waldeisen JR, Juluri BK, Huang TJ. Lab Chip. 2007; 7:1303. [PubMed: 17896014]

29. Shi J, Mao X, Ahmed D, Colletti A, Huang TJ. Lab Chip. 2008; 8:221. [PubMed: 18231658]

30. Shi J, Huang H, Stratton Z, Lawit A, Huang Y, Huang TJ. Lab Chip. 2009; 9:3354. [PubMed: 19904400]

31. Ahmed D, Mao X, Juluri BK, Huang TJ. Microfluid Nanofluid. 2009; 7:727.

32. Shi J, Ahmed D, Mao X, Lin SS, Huang TJ. Lab Chip. 2009; 9:2890. [PubMed: 19789740]

33. Mao X, Lin SS, Lapsley MI, Shi J, Juluri BK, Huang TJ. Lab Chip. 2009; 9:2050. [PubMed: 19568674]

34. Ahmed D, Mao X, Shi J, Juluri BK, Huang TJ. Lab Chip. 2009; 9:2738. [PubMed: 19704991]

35. Novoselov KS, Geim AK, Morozov SV, Jiang D, Zhang Y, Dubonos SV, Grigorieva IV, Firsov AA. Science. 2004; 306:666. [PubMed: 15499015]

36. Mohanty N, Berry V. Nano Lett. 2008; 8:4469. [PubMed: 19367973]

37. Wu P, Shao QA, Hu YJ, Jin JA, Yin YJ, Zhang H, Cai CX. Electrochimica Acta. 2010; 55:8606.

38. Schedin F, Geim AK, Morozov SV, Hill EW, Blake P, Katsnelson MI, Novoselov KS. Nat Mater. 2007; 6:652. [PubMed: 17660825]

39. Ling X, Xie LM, Fang Y, Xu H, Zhang HL, Kong J, Dresselhaus MS, Zhang J, Liu ZF. Nano Letters. 2010; 10:553. [PubMed: 20039694]

40. Yu XX, Cai HB, Zhang WH, Li XJ, Pan N, Luo Y, Wang XP, Hou JG. ACS Nano. 2011; 5:952. [PubMed: 21210657]

41. Ren W, Fang YX, Wang EK. ACS Nano. 2011; 5:6425. [PubMed: 21721545]

42. Lu G, Li H, Liusman C, Yin ZY, Wu SX, Zhang H. Chem Sci. 2011; 2:1817.

43. Liu CY, Liang KC, Chen W, Tu CH, Liu CP, Tzeng Y. Opt Express. 2011; 19:17092. [PubMed: 21935070]

44. Liu CY, Liang KC, Chen WL, Tu CH, Liu CP, Tzeng Y. ACS Appl Mater Interfaces. 2011; 3:2944. [PubMed: 21728327]

45. Zhang Z, Xu F, Yang W, Guo M, Wang X, Zhang B, Tang J. Chem Commun. 2011; 47:6440.

46. Fu XQ, Bei FL, Wang X, O'Brien S, Lombardi JR. Nanoscale. 2010; 2:1461. [PubMed: 20820735]

47. Mahajan S, Cole RM, Speed JD, Pelfrey SH, Russell AE, Bartlett PN, Barnett SM, Baumberg JJ. J Phys Chem C. 2010; 114:7242.

48. Wang YY, Ni ZH, Hu HL, Hao YF, Wong CP, Yu T, Thong JTL, Shen ZX. Appl Phys Lett. 2010; 97:163111.

49. Kim J, Cote LJ, Kim F, Huang JX. J Am Chem Soc. 2010; 132:260. [PubMed: 19961229]

50. Colombo L, Li XS, Cai WW, An JH, Kim S, Nah J, Yang DX, Piner R, Velamakanni A, Jung I, Tutuc E, Banerjee SK, Ruoff RS. Science. 2009; 324:1312. [PubMed: 19423775]

51. Colombo L, Li XS, Cai WW, Ruoff RS. Nano Lett. 2009; 9:4268. [PubMed: 19711970]

52. Hao QZ, Zeng Y, Wang XD, Zhao YH, Wang B, Chiang IK, Werner DH, Crespi V, Huang TJ. Appl Phys Lett. 2010; 97:193101.

53. Swan AK, Metzger C, Remi S, Liu MK, Kusminskiy SV, Neto AHC, Goldberg BB. Nano Lett. 2010; 10:6. [PubMed: 19928908]

54. Kim K, Lee Z, Regan W, Kisielowski C, Crommie MF, Zettl A. ACS Nano. 2011; 5:2142. [PubMed: 21280616]

55. Muller DA, Huang PY, Ruiz-Vargas CS, van der Zande AM, Whitney WS, Levendorf MP, Kevek JW, Garg S, Alden JS, Hustedt CJ, Zhu Y, Park J, McEuen PL. Nature. 2011; 469:389. [PubMed: 21209615]

56. Lee J, Novoselov KS, Shin HS. ACS Nano. 2011; 1:608. [PubMed: 21174405]

57. Schedin F, Lidorikis E, Lombardo A, Kravets VG, Geim AK, Grigorenko AN, Novoselov KS, Ferrari AC. ACS Nano. 2010; 4:5617. [PubMed: 20857921]

58. Tang W, Xu H, Park EJ, Philbert MA, Kopelman R. Biochem Biophys Res Commun. 2008; 369:579. [PubMed: 18298950]

59. Folkes LK, Wardman P. Cancer Res. 2003; 63:776. [PubMed: 12591725]

60. Sougata Sarkar SP, Subhra J, Arun KS, Mukul P, Mrinmoyee BJC, Tarasankar P. J Phys Chem C. 2008; 112:17862.

61. Xu H, Xie LM, Zhang HL, Zhang J. ACS Nano. 2011:5338. [PubMed: 21678950]

62. Wehling TO, Novoselov KS, Morozov SV, Vdovin EE, Katsnelson MI, Geim AK, Lichtenstein AI. Nano Lett. 2008; 8:173. [PubMed: 18085811]

63. Ling X, Zhang J. Small. 2010; 6:2020. [PubMed: 20730826]

64. Morton SM, Jensen L. J Am Chem Soc. 2009; 131:4090. [PubMed: 19254020]

65. Qiu C, Zhou H, Yang H, Chen MG, Sun YL. J Phys Chem C. 2011; 115:10019.

66. Haes AJ, Haynes CL, McFarland AD, Schatz GC, Van Duyne RR, Zou SL. MRS Bull. 2005; 30:368.

67. de Abajo FJG. Rev Mod Phys. 2007; 79:1267.

68. Liu YJ, Hao QZ, Smalley JST, Liou J, Khoo IC, Huang TJ. Appl Phys Lett. 2010; 97:091101.

69. Hao QZ, Zhao YH, Juluri BK, Kiraly B, Liou J, Khoo IC, Huang TJ. J Appl Phys. 2011; 109:084340.

70. Zheng YB, Huang TJ, Desai AY, Wang Tan SJL, Gao KH, Huan ACH. Appl Phys Lett. 2007; 90:183117.

71. Zheng YB, Jensen L, Yan W, Walker TR, Juluri BK, Jensen L, Huang TJ. J Phys Chem C. 2009; 113:7019.

72. Hiep HM, Yoshikawa H, Saito M, Tamiya E. ACS Nano. 2009; 3:446. [PubMed: 19236084]

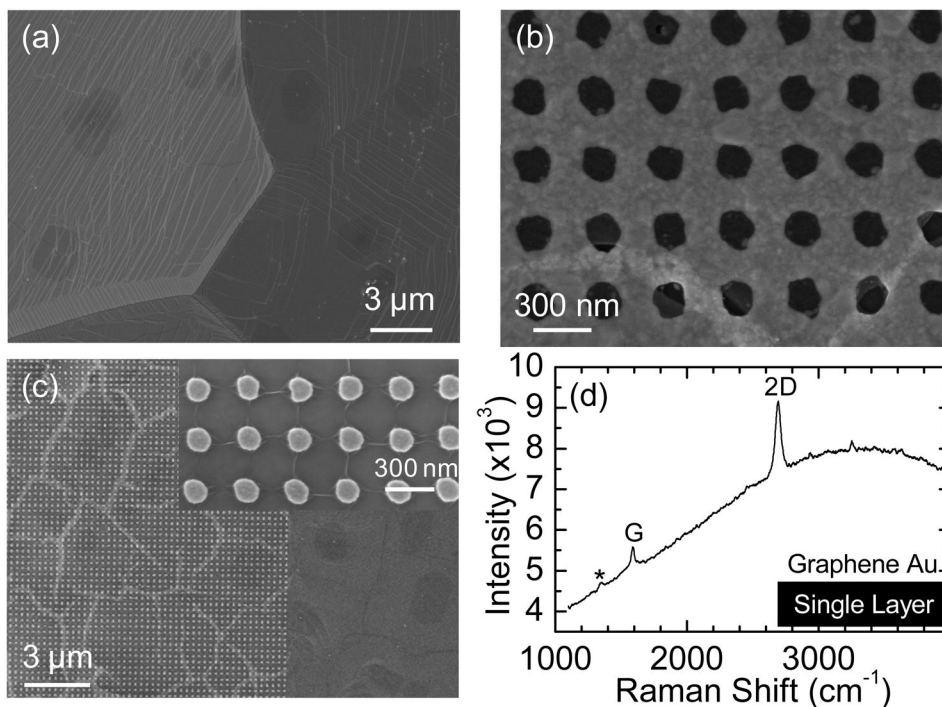73. Eibert TF, Volakis JL, Wilton DR, Jackson DR. IEEE T Antenn Propag. 1999; 47:843.

Figure 1.
(a) Scanning electron microscope (SEM) image of as-grown graphene on copper foil. (b) SEM images of transferred graphene on nanoholes fabricated on a glass substrate. A crack in the graphene near the bottom of the image is intentionally shown. (c) SEM images of transferred graphene on nanoparticles fabricated on a silicon wafer with 290 nm thermal oxide. The graphene cracks are presumably along domain boundaries. Wrinkles are formed in the lattice's direction within each domain, as shown in the inset. (d) Raman spectrum of transferred graphene on Au nanoholes using a 514 nm laser with a power of ~ 2mW/μm^2 on sample, 10 second integration time, and one accumulation. A very small D band is marked by *.
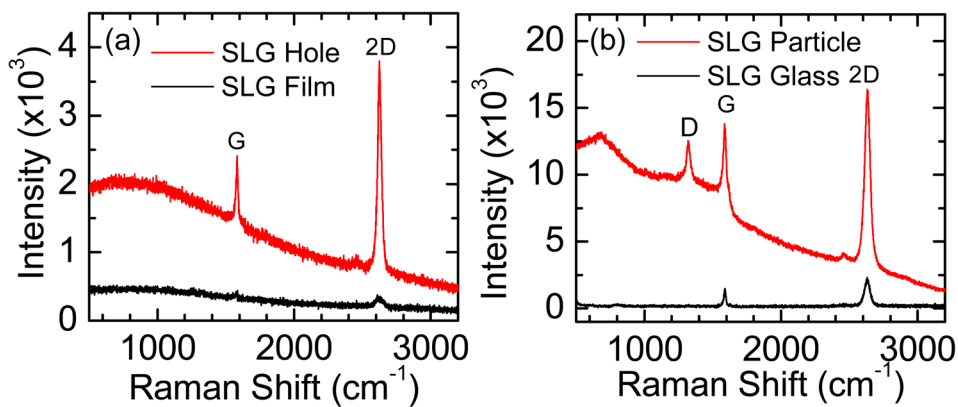
Figure 2.
(a) Raman spectra of transferred graphene on Au film and Au nanoholes. (b) Raman spectra of transferred graphene on Au nanoparticles and glass. Both Raman measurements are performed with a 647 nm laser with a power of ~ 1mW/μm^2 on sample, 10 second integration time, and one accumulation.
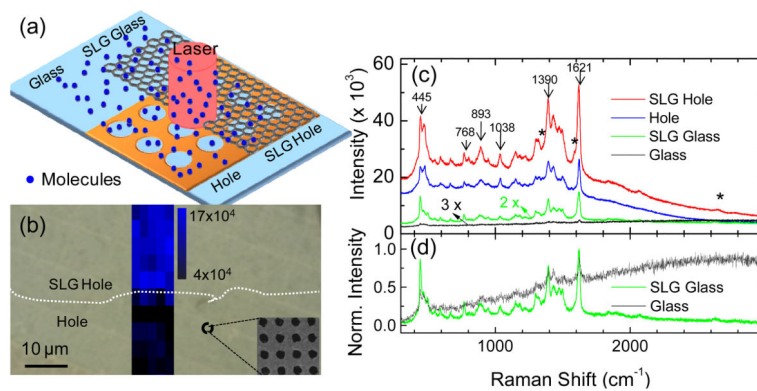
Figure 3.

(a) Schematic of a graphene and nanohole system. Four different areas of the substrate are shown. (b) Raman mapping of 1621 cm^{-1} methylene blue peak at the graphene edge on the nanohole array overlaying an optical micrograph of the sample. Graphene is not visible without interference effect. The dotted line shows the graphene border, as confirmed by SEM. (c) Raman spectra of methylene blue on four different areas of the substrate: glass, graphene-covered glass, Au nanoholes, and graphene-covered Au nanoholes. (d) Raman spectra for glass and graphene-glass areas, normalized to maximum intensity. The D band, G band and 2D band of graphene are indicated by *. All Raman measurements are performed with a 647 nm laser with a power of ~ 1mW/μm^2 on sample, 10 second integration time, and one accumulation.
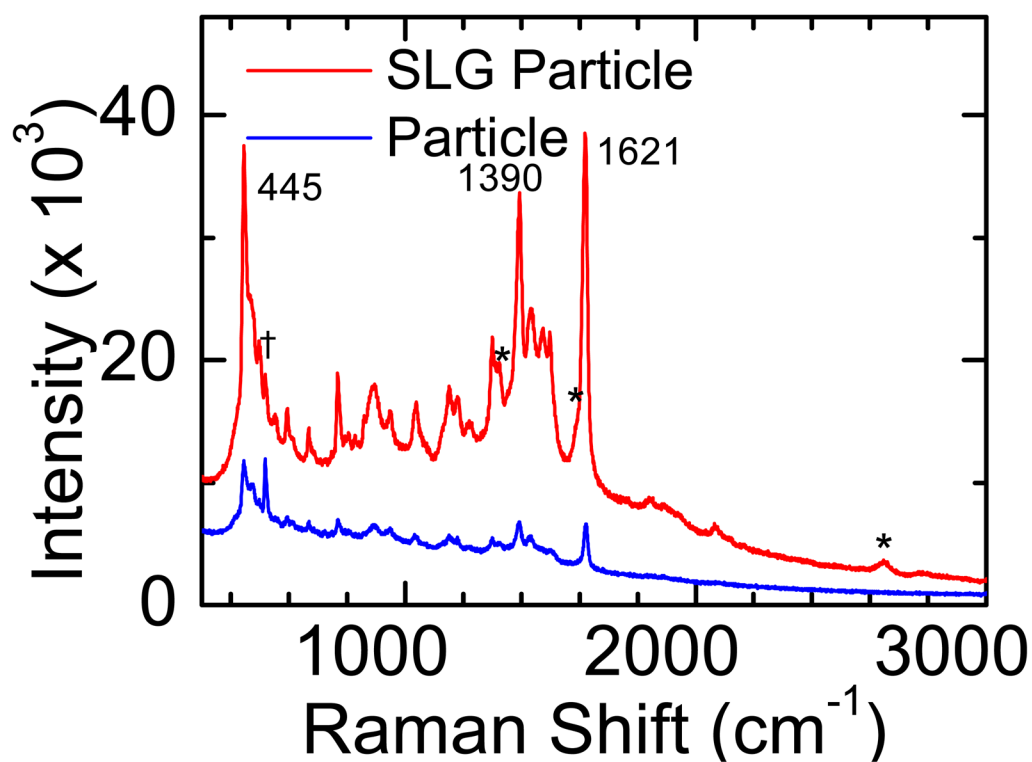
Figure 4.
Raman spectra of methylene blue on nanoparticles and on graphene covered nanoparticles. The D band, G band and 2D band of graphene are indicated by *, and the Raman peak marked by † comes from the silicon substrate. Both Raman measurements are performed with a 647 nm laser with a power of ~ 1mW/μm² on sample, 10 second integration time, and one accumulation.
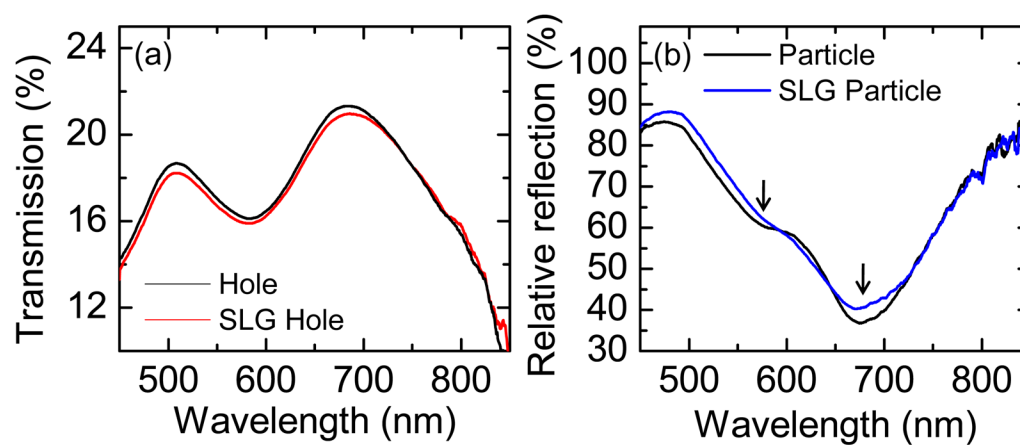
Figure 5.
(a) Transmission spectra of Au nanohole array with or without graphene. (b) Relative reflection spectra of the Au nanoparticle array on Si wafer with or without graphene.
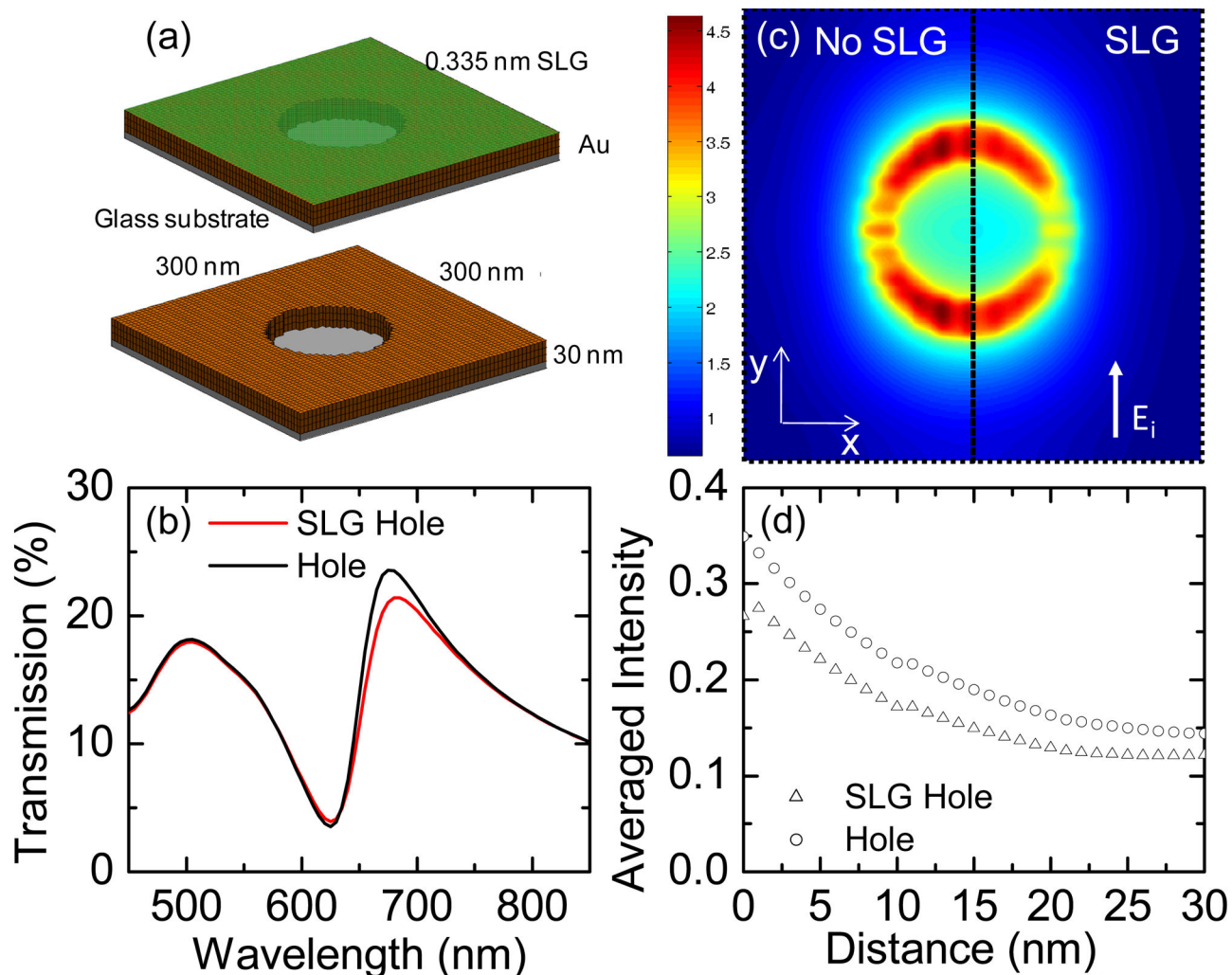
Figure 6.
Comparative simulations of nanohole array with and without graphene. (a) The simulated nanohole geometry. (b) Simulated transmission spectra. (c) Electric field intensity distributions 1 nm above the Au surface under a 660 nm incident wave polarized in the y-direction. The left half, without graphene, and right half, with graphene. (d) Distance-dependent averaged electric field intensity in a unit cell away from the structure surface (distance = 0 nm at the Au surface) into the air. Intensity is plotted on a logarithmic scale.